Absorption spectra of H_2-H_2 pairs in the fundamental band

Wilfried Meyer
Fachbereich Chemie der Universität, D-6750 Kaiserslautern, Federal Republic of Germany

Aleksandra Borysow*
Joint Institute for Laboratory Astrophysics, University of Colorado, Boulder, Colorado 80309-0440

Lothar Frommhold
Physics Department, University of Texas at Austin, Austin, Texas 78712-1081
(Received 26 June 1989)

For the computation of the induced-dipole moment, the collisional complex consisting of two H_2 molecules is treated like one molecule in the self-consistent-field and size-consistent, coupled electron pair approximations that separates correctly at distant range. The basis set accounts for 95% of the correlation energies. The radial transition matrix elements of the induced-dipole components are obtained for the two cases $v_1=v_2=0$ and $v_1=0, v_2=1$, where the v_i are the vibrational quantum numbers of the interacting H_2 molecules ($i=1$ or 2). The dependence of these elements on the most important rotational states $(j_1, j_1', j_2, j_2'=0, \ldots, 3)$ involved is obtained and seen to be significant in the fundamental band. The results are recast in a simple, but accurate analytical form that is used in a quantum formalism for computations of the spectral moments (sum rules) and line shapes of the collision-induced absorption spectra of molecular hydrogen pairs in the infrared 2.4-μm band. The calculations are based on a proven isotropic potential model that we have extended to account for effects of vibrational excitations. Numerical consistency of the line-shape calculations with the sum rules is observed at the 1% level. The comparison of the computational results with the available measurements at temperatures from 20 to 300 K shows agreement within the estimated uncertainties of the best measurements ($\approx 10\%$). This fact suggests that theory is capable of predicting these spectra reliably at temperatures for which no measurements exist, with an accuracy that compares favorably with that of good laboratory measurements.

I. INTRODUCTION

Homonuclear molecules likes hydrogen are nonpolar and hence infrared inactive. Welsh and co-workers have shown, however, that compressed gases composed of atoms and/or nonpolar molecules absorb infrared radiation due to dipole moments induced by molecular interactions.[1] The details of such collision-induced absorption (CIA) are now well understood.[1-4] Extensive literature on collision-induced spectra exists and has been compiled in a bibliography and update.[5,6] Current interest in the modeling of radiative transfer in the atmospheres of the planets and cool stars requires accurate knowledge of the temperature dependence of a number of rotovibrational spectral profiles of various systems, especially those containing hydrogen.[1,7-10]

Theoretical profiles of CIA spectra have been computed from first principles for years.[11,12] Once reliable intermolecular interaction potentials became available[13] and the calculations of the induced-dipole moments had reached the perfection that is now observed,[14] accurate computations of the rototranslational (RT) CIA spectra became routine. Remarkably good agreement of measured and *ab initio* computed RT spectra was observed for a number of simple systems.[15-20] We note that for the more highly polarizable systems, a useful theoretical approximation of the observed RT spectra is possible with the use of the classical multipole–induced-dipole model[21,22] if good interaction potentials are employed. Recently, rotovibrational (RV) spectra were also computed from first principles, using advanced quantum chemical methods;[23,24] the H_2-He complex was an obvious choice for that study. In contrast to the somewhat uneventful studies of the RT spectra, for a successful modeling of RV spectra several novel effects had to be considered that were of little or no significance for RT spectra.

It has been known for some time that vibrational excitation of a molecule (H_2) affects the intermolecular interactions.[13,25,26] For the computation of the RV spectra, the final state of the pair H_2-X (where X stands for He, H_2, or most anything else) interacts through a potential that differs from that of the initial state; the differences are substantial, especially at near range (repulsive core) where the spectroscopic interactions take place. In line-shape computations, interaction potentials of initial and final states are important and the proper accounting for the vibrational dependences leads to line shapes that, perhaps surprisingly, differ discernibly from those computed with the assumption of identical interactions for initial and final states.[23] A related theoretical study[27] pointed out how the RV line profiles $G(\omega)$ deviate from

 ©1989 The American Physical Society

the symmetry that is so familiar from RT studies,

$$G(-\omega)=\exp(-\hbar\omega/kT)G(\omega) \quad (1)$$

("principle of detailed balance"). For the RV line profiles, this relation is modified significantly.[27] As a consequence, most spectral moments, especially the odd ones, are affected significantly by the details of the variation of the interaction with vibrational excitation;[28] for example, the use of existing sum formulas that do not account for the vibration dependence of the H_2-He potential renders the first moments too small by about 25% at 300 K, and more at higher temperatures. Finally, in the vibrational band, the radial induced-dipole matrix elements show a dependence on the rotational transitions involved that cannot be ignored.[24] We note that for the RT matrix elements, this dependence amounts to only a $\approx 1\%$ correction for the most important rotational lines which may be safely neglected in most cases. The effects of the variations of the interaction potential due to vibration and the rotational dependences of the induced dipole moment on the RV CIA spectra of H_2-H_2 pairs cannot be ignored and will be considered in this work.

The work presents the induced-dipole components of H_2-H_2 pairs as function of the molecular orientations and the intra- and intermolecular separations, along with their RV radial matrix elements of transitions involving vibrational excitation of one molecule, $v_2=0\rightarrow v_2'=1$ and $j_1,j_1',j_2,j_2'=0$, 1, 2, and 3. These data are computed from highly correlated wave functions, with an estimated numerical precision of better than 3%, and are employed to compute the RV CIA spectra of H_2 pairs in the fundamental band. To that end, the vibrational dependences of the isotropic part of the H_2-H_2 interaction potential are obtained from first principles. The results are compared to existing measurements at temperatures from 20 to 300 K; we shall see close agreement.

II. THE *AB INITIO* INDUCED DIPOLE

Early attempts to calculate the induced-dipole moment of H_2-H_2 pairs from first principles are known.[29–35] van Kranendonk observes that "especially for H_2" accurate *ab initio* calculations would be "very useful."[2] The most detailed previous computations[32–35] are limited to small separations and to an internuclear distance of the H_2 molecules of 1.401 bohrs. Near the separation of $R=4.5$ bohrs, these computations are in reasonable agreement with the quadrupole-induced component but depart rapidly from it with increasing separation R. Only in recent times, it seems, could the substantial problems of such computations be controlled and very precise data be generated.[14]

Collisionally-induced-dipole moments arise from three mechanisms: polarization in the static multipole field of a collisional partner, induction by overlap, and by dispersion forces. As was previously pointed out,[14] their *ab initio* calculation poses problems similar to those known from the calculation of van der Waals potentials. For the spectroscopically most relevant molecular separations, i.e., around the collision diameter, the induced moments are rather small, but perturbation theory fails to adequately handle the exchange contribution which become large at such short distances. We have, therefore, treated the H_2-H_2 complex as a supermolecule in self-consistent-field (SCF) and configuration-interaction (CI) calculations, and taken care that the basis set superposition error is effectively controlled and the CI excitation level is adequate for the long-range effects.

It was shown previously[14,16,17] that a standard singles plus doubles CI (or corresponding pair treatment) is insufficient for systems involving H_2. This is due to the fact that the quadrupole moment of H_2 is in error by 8% for an SCF wave function, and by 4% if the SCF orbital is replaced by the principal natural orbit. Thus H_2 has to be described by a wave function including the leading double substitutions, and the proper inductive response of the collisional partner requires either triple substitutions or a multiconfiguration (MC) reference CI. Our recent calculations[14,16,17] of systems containing H_2 have been based on the latter method. However, when extending the set of molecular geometries for H_2-H_2 to one of no symmetry and short separations, we encountered problems with a stable definition of localized orthogonal MC SCF orbitals, resulting in numerical noise for the smaller components of the induced-dipole components. For the present calculations we have, therefore, adopted the alternative procedure of including triple substitutions with respect to the SCF wave functions. The main dipole components appear to be affected little by this change of computational procedure. In all other aspects, our present calculations follow the procedures used in Refs. 14 and 16–18.

The basis set of Gaussian-type functions used here is identical to the set given in Table I of Ref. 16. This mixed two-center–one-center basis has been designed to account accurately for the properties of H_2 pertinent here, i.e., its low-order multipole moments q_2 and q_4 and the polarizability invariants α and γ. This is shown in Table I which compares previous results[36,37] (a) with our present results (b). The values (b) refer to calculations performed for a H_2 bond distance of $\langle r\rangle=1.449$ bohrs, the mean bond distance for zero point vibration. As we have argued in our earlier work on van der Waals coefficients,[25] using this distance effectively accounts for zero-point vibrational averaging. Indeed, when investigating collision-induced vibrational excitations in the H_2-He system,[23] we could compare zero-point-averaged dipoles obtained from a dipole fit to values at three H_2 bond distances with the ones computed at the mean distance $\langle r\rangle$. The differences are less than 1% for large intermolecular separations and remain below 2% even at very short distances.[16] For the specified basis, superposition errors are in the order of 1%, but they are effectively excluded by projecting the correlation orbitals for intramolecular electron pairs onto the local molecular basis. We further note that calculations with various extended basis sets did not lead to dipole moment changes larger than 1%.

The induced dipole moment $\boldsymbol{\mu}$ is expressed in the form of its spherical components, μ_ν with $\nu=0,\pm1$, which are related to the Cartesian components by $\mu_0=\mu_z$,

$\mu_{\pm 1}=\mp(\mu_x \pm i\mu_y)/\sqrt{2}$. We write[38–41]

$$\mu_\nu(R,r_1,r_2,\Omega_1,\Omega_2,\Omega) = \frac{(4\pi)^{3/2}}{\sqrt{3}} \sum_{\lambda_1,\lambda_2,\Lambda,L} A_{\lambda_1\lambda_2\Lambda L}(R,r_1,r_2) \times Y^{1\nu}_{\lambda_1\lambda_2\Lambda L}(\Omega_1,\Omega_2,\Omega) , \quad (2)$$

with real coefficients A. The function $Y^{1\nu}_{\lambda_1\lambda_2\Lambda L}$ is given in terms of spherical harmonics as

$$Y^{1\nu}_{\lambda_1\lambda_2\Lambda L}(\Omega_1,\Omega_2,\Omega) = \sum_{M,M_1,M_2,M_\Lambda} Y_{\lambda_1 M_1}(\Omega_1) Y_{\lambda_2 M_2}(\Omega_2) Y_{LM}(\Omega) \times C(\lambda_1\lambda_2\Lambda; M_1 M_2 M_\Lambda) \times C(\Lambda L 1; M_\Lambda M \nu) . \quad (3)$$

The quadrupole sum reduces to a double sum at once because Clebsch-Gordan coefficients $C(\,)$ vanish unless $M_1+M_2=M_\Lambda$ and $M_\Lambda+M=\nu$. The quantities Ω_i represent the orientations of the internuclear axes of molecules $i=1$ and 2 and Ω designates the orientation of the vector joining the molecular centers of mass. The parameters $\lambda_1, \lambda_2, \Lambda$, and L are all non-negative integers.

Due to the inversion symmetry of the H_2 molecule, only even λ_1 and λ_2 occur. Moreover, from parity considerations it follows that $\lambda_1+\lambda_2+L$ is odd. In conjunction with the triangular inequality conditions imposed by the Clebsch-Gordan coefficients, Eq. (3), we have

$$|\lambda_1-\lambda_2| \le \Lambda \le \lambda_1+\lambda_2, \quad |L-1| \le \Lambda \le L+1 ; \quad (4)$$

furthermore, $\lambda_1+\lambda_2 \ge \Lambda$. For identical molecules 1 and 2, this amounts to $\Lambda=L\pm 1$ if $\lambda_1 \neq \lambda_2$, and $\Lambda=L$ if $\lambda_1=\lambda_2$, but if the two H_2 molecules have different bond distances, additional terms such as the isotropic overlap ($\lambda_1\lambda_2\Lambda L=0001$) occur.

Starting from a set of 13 relative orientations of the H_2-H_2 pair, we found that the 11 leading terms of Eq. (2) could be determined with sufficient numerical significance, namely, the $A_{\lambda_1\lambda_2\Lambda L}(R;r_1,r_2)$ with the subscripts

$$\lambda_1\lambda_2\Lambda L = 0001,\ 2023,\ 0223,\ 2021,\ 0221,\ 2233,\ 2211,\ 4045,\ 0445,\ 2245,\ \text{and}\ 2243 . \quad (5)$$

The last two of these are already smaller than the leading terms ($\lambda_1\lambda_2\Lambda L=0001$, 0223, and 2023) by nearly two orders of magnitude. These terms and higher ones can safely be neglected.

Our final set of calculations has been performed for the 13 nonequivalent orientations that are indicated in the first line of Table II. The ϑ_i are the angles subtended by the vectors $\hat{\mathbf{r}}_i$ and $\hat{\mathbf{R}}$, and $\Delta\varphi$ is the dihedral angle defined by the planes $\hat{\mathbf{r}}_1,\hat{\mathbf{R}}$ and $\hat{\mathbf{r}}_2,\hat{\mathbf{R}}$. These angles assume values

TABLE I. Pertinent properties of H_2 molecules and H_2-H_2 pairs, in atomic units. Upper lines: previous results (Refs. 36 and 37); A elements calculated from Eq. (11) from H_2 properties. Lower lines: this work, H_2; obtained from calculations at $r_0, r_\pm$, A coefficients from the long-range fits, see Tables V and VI.

		Previous results				
P	$P(r_0)$	$\langle 0\|P\|0\rangle$	$\langle 0\|P\|1\rangle$	$\langle 0\|P\|\bar{0}\rangle$	$\langle 0\|P\|\bar{1}\rangle$	$\langle \bar{0}\|P\|1\rangle$[a]
α		5.4138	0.7392	0.0024	−0.0176	0.0181
	5.380	5.3945	0.7199	0.0023	−0.0175	0.0179
γ		2.0238	0.6100	0.0020	−0.0065	0.0074
	1.9920	2.0355	0.5897	0.0019	−0.0066	0.0073
q_2		0.4835	0.0879	0.0003	−0.0016	0.0016
	0.4773	0.4783	0.0887	0.0003	−0.0016	0.0016
q_4		0.353	0.1451	0.0005	−0.0012	0.0012
	0.3326	0.3532	0.1539	0.0005	−0.0011	0.0014

		This work				
	$A(r_0,r_0)$	$\langle 00\|A\|00\rangle$	$\langle 00\|A\|01\rangle$	$\langle 00\|A\|0\bar{0}\rangle$	$\langle 00\|A\|0\bar{1}\rangle$	$\langle 0\bar{0}\|A\|01\rangle$
2023		4.5338	0.6190	0.0020	−0.0147	0.0152
	4.53	4.56	0.622	0.0021	−0.0148	0.0152
0223		−4.5338	−0.8242	−0.0028	0.0150	−0.0150
	−4.53	−4.56	−0.853	−0.0028	0.0149	−0.0154
2233		−0.6916	−0.1727	−0.0005	−0.0023	0.0025
	−0.687	−0.702	−0.163	−0.0005	0.0023	−0.0024
4045		4.2733	0.5835	0.0019	−0.0139	0.0143
	4.42	4.62	0.779	0.0028	−0.0176	0.0176
0445		−4.2733	−1.7565	−0.0061	0.0145	−0.0148
	−4.42	−4.62	−2.20	−0.0072	0.0170	−0.0195

[a] $\langle 0|P|\bar{1}\rangle = (\langle 00|P|1j\rangle - \langle 00|P|10\rangle)/[j(j+1)]$, see text.

TABLE II. Cartesian dipole moment components in 10^{-6} a.u., for three bond distances, $r_0=1.449$ bohr, $r_-=1.111$ bohr, $r_+=1.787$ bohr, and 13 relative orientations, $(\angle\vartheta_1,\vartheta_2,\Delta\varphi)$: number 0 means 0°, 1 means 45°, 2 means 90°, 3 means 135°, respectively.

R (bohr)	∠020	∠200	∠030	∠300	∠230	∠120	∠122	∠232	∠130	∠000	∠220	∠222	∠110
						$\mu_x(r_0r_0)$							
3.5	0	0	−9602	−9602	−8694	−8694	−1290	−1290	−18419	0	0	0	0
4.0	0	0	−8858	−8858	−7927	−7927	−3276	−3276	−16774	0	0	0	0
4.5	0	0	−7404	−7404	−6552	−6552	−3498	−3498	−13935	0	0	0	0
5.0	0	0	−5869	−5869	−5143	−5143	−3065	−3065	−11000	0	0	0	0
5.5	0	0	−4519	−4519	−3932	−3932	−2474	−2474	−8444	0	0	0	0
6.0	0	0	−3436	−3436	−2972	−2972	−1923	−1923	−6404	0	0	0	0
7.0	0	0	−1983	−1983	−1703	−1703	−1125	−1125	−3684	0	0	0	0
8.0	0	0	−1182	−1182	−1011	−1011	−669	−669	−2192	0	0	0	0
9.0	0	0	−739	−739	−631	−631	−416	−416	−1369	0	0	0	0
						$\mu_z(r_0r_0)$							
3.5	133881	−133881	73235	−73235	−61181	61181	60809	−60809	0	0	0	0	0
4.0	75776	−75776	41905	−41905	−34438	34438	34326	−34326	0	0	0	0	0
4.5	43444	−43444	23975	−23975	−19822	19822	19791	−19791	0	0	0	0	0
5.0	25834	−25834	14120	−14120	−11897	11897	11891	−11891	0	0	0	0	0
5.5	16167	−16167	8731	−8731	−7529	7529	7530	−7530	0	0	0	0	0
6.0	10652	−10652	5685	−5685	−5015	5015	5017	−5017	0	0	0	0	0
7.0	5272	−5272	2760	−2760	−2527	2527	2529	−2529	0	0	0	0	0
8.0	2973	−2973	1537	−1537	−1441	1441	1442	−1442	0	0	0	0	0
9.0	1824	−1824	935	−935	−890	890	891	−891	0	0	0	0	0
						$\mu_x(r_0r_-)$							
3.5	0	0	−8355	−5138	−7854	−4432	−262	−3336	−12941	0	0	0	3300
4.0	0	0	−6632	−5810	−6245	−4999	−2422	−3377	−11846	0	0	0	1036
4.5	0	0	−5116	−5194	−4790	−4447	−2779	−2894	−9773	0	0	0	139
5.0	0	0	−3859	−4226	−3594	−3600	−2479	−2297	−7640	0	0	0	−181
5.5	0	0	−2876	−3289	−2668	−2788	−2009	−1756	−5811	0	0	0	−261
6.0	0	0	−2138	−2510	−1980	−2118	−1562	−1322	−4373	0	0	0	−251
7.0	0	0	−1205	−1451	−1115	−1215	−912	−751	−2493	0	0	0	−171
8.0	0	0	−713	−865	−660	−721	−543	−445	−1480	0	0	0	−106
9.0	0	0	−445	−541	−413	−449	−338	−277	−924	0	0	0	−66
						$\mu_z(r_0r_-)$							
3.5	133215	−49149	101606	2170	−14932	68640	68565	−14737	36457	66207	15884	15993	37969
4.0	72501	−29437	54027	−1720	−9609	37091	37101	−9529	18319	33015	8174	8239	19348
4.5	39901	−18297	28752	−2901	−6573	20258	20280	−6536	8992	16125	3999	4038	9670
5.0	22627	−11996	15603	−3038	−4789	11333	11352	−4771	4284	7768	1779	1803	4731
5.5	13445	−8279	8812	−2756	−3628	6597	6611	−3618	1974	3726	662	678	2271
6.0	8438	−5928	5252	−2319	−2784	4046	4056	−2779	879	1806	152	162	1081
7.0	3905	−3266	2235	−1482	−1656	1807	1811	−1654	155	472	−123	−119	254

TABLE II. (*Continued*).

R (bohr)	∠020	∠200	∠030	∠300	∠230	∠120	∠122	∠232	∠130	∠000	∠220	∠222	∠110
8.0	2142	−1926	1175	−912	−1005	978	980	−1005	23	171	−117	−115	78
9.0	1304	−1200	705	−572	−633	595	596	−633	3	89	−81	−80	36
						$\mu_x(r_0r_+)$							
3.5	0	0	−7337	−15 532	−6878	−13 565	−2419	4040	−21 957	0	0	0	−7270
4.0	0	0	−9551	−12 586	−8324	−11 292	−4154	−1555	−20 865	0	0	0	−2935
4.5	0	0	−9067	−9959	−7688	−8978	−4218	−3289	−17 802	0	0	0	−1075
5.0	0	0	−7688	−7704	−6400	−6931	−3650	−3429	−14 335	0	0	0	−276
5.5	0	0	−6169	−5868	−5068	−5265	−2937	−2995	−11 169	0	0	0	44
6.0	0	0	−4816	−4440	−3916	−3973	−2284	−2430	−8564	0	0	0	151
7.0	0	0	−2859	−2553	−2288	−2278	−1337	−1474	−4986	0	0	0	153
8.0	0	0	−1721	−1518	−1364	−1356	−795	−884	−2978	0	0	0	103
9.0	0	0	−1079	−947	−849	−847	−495	−550	−1861	0	0	0	66
						$\mu_z(r_0r_+)$							
3.5	130 553	−258 518	27 486	−188 165	−122 173	51 943	51 035	−121 537	−50 800	−106 898	−16 327	−16 628	−54 381
4.0	76 953	−144 368	21 268	−103 802	−67 318	30 699	30 339	−67 208	−25 591	−54 852	−8713	−8894	−28 144
4.5	45 796	−80 445	15 130	−56 274	−37 464	18 633	18 481	−37 487	−12 618	−26 759	−4531	−4640	−14 352
5.0	28 364	−45 925	10 728	−30 867	−21 412	11 967	11 899	−21 457	−6071	−12 774	−2185	−2253	−7225
5.5	18 540	−27 367	7803	−17 536	−12 740	8178	8145	−12 778	−2820	−6003	−917	−960	−3587
6.0	12 704	−17 153	5786	−10 458	−7953	5841	5823	−7981	−1249	−2787	−290	−319	−1765
7.0	6627	−7837	3294	−4388	−3608	3228	3223	−3622	−186	−589	98	86	−436
8.0	3823	−4239	1950	−2262	−1950	1917	1916	−1957	4	−142	125	119	−131
9.0	2365	−2554	1209	−1335	−1178	1204	1203	−1182	25	−50	96	93	−54
						$\mu_x(r_-r_+)$							
3.5	0	0	−2903	−12 265	−1587	−11 167	−4308	4639	−13 629	0	0	0	−9749
4.0	0	0	−5738	−9053	−4634	−8534	−4098	−836	−13 983	0	0	0	−3582
4.5	0	0	−6176	−6755	−4998	−6432	−3455	−2565	−12 181	0	0	0	−1015
5.0	0	0	−5463	−5020	−4400	−4795	−2734	−2779	−9844	0	0	0	9
5.5	0	0	−4455	−3717	−3568	−3557	−2092	−2450	−7654	0	0	0	360
6.0	0	0	−3499	−2756	−2786	−2643	−1579	−1992	−5846	0	0	0	432
7.0	0	0	−2082	−1548	−1638	−1494	−899	−1208	−3383	0	0	0	332
8.0	0	0	−1254	−912	−976	−887	−532	−725	−2015	0	0	0	212
9.0	0	0	−786	−567	−607	−555	−331	−451	−1258	0	0	0	134
						$\mu_z(r_-r_+)$							
3.5	39 276	−244 824	−48 025	−208 202	−122 686	2119	1674	−122 609	−84 746	−168 238	−31 975	−32 321	−89 138
4.0	25 668	−132 185	−20 372	−109 753	−65 837	3429	3221	−65 928	−42 776	−84 654	−16 794	−17 000	−45 834
4.5	17 309	−71 374	−7407	−57 273	−35 479	3812	3708	−35 573	−21 159	−41 362	−8484	−8608	−23 200

TABLE II. (*Continued*).

R (bohr)	∠020	∠200	∠030	∠300	∠230	∠120	∠122	∠232	∠130	∠000	∠220	∠222	∠110
5.0	12 323	−39 341	−1504	−30 151	−19 398	3843	3787	−19 467	−10 201	−19 917	−3940	−4018	−11 550
5.5	9169	−22 534	982	−16 323	−10 905	3596	3564	−10 952	−4760	−9513	−1571	−1621	−5657
6.0	6958	−13 575	1809	−9236	−6398	3138	3119	−6428	−2138	−4544	−440	−472	−2744
7.0	4098	−5833	1692	−3530	−2607	2112	2105	−2621	−364	−1096	219	205	−662
8.0	2481	−3068	1143	−1735	−1333	1340	1337	−1340	−37	−347	239	232	−199
9.0	1563	−1833	737	−1010	−790	860	858	−793	10	−162	175	172	−85

of 0°, 45°, 90°, and 135°, which are marked in the table by the numbers 0, 1, 2, and 3, respectively. This set provides 8 nonredundant Cartesian dipole components if $r_1 = r_2$, and 21 components if $r_1 \neq r_2$. The dipole components are collected in Table II for four nonredundant pairs of bond distances and nine intermolecular separations.

From the Cartesian dipole components, Table II, the spherical tensor components $A_{\lambda_1\lambda_2\Lambda L}(R;r_1r_2)$ are obtained by solving Eqs. (2) for the A coefficients by least-squares techniques. (The results are not shown). These are represented by quadratic polynomials in the bond distance. From these, the radial transition matrix elements

$$B^{(s)}_{(c)}(R) = \langle v_1 j_1 v_2 j_2 | A_{(c)}(R;r_1r_2) | v_1' j_1' v_2' j_2' \rangle \qquad (6)$$

are obtained at once with the help of the radial matrix elements $\langle vj|r^n|v'j'\rangle$ which we compute for $n = 0, \ldots, 3$ from the well-known H-H interaction potential.[42–44] As a result, we obtain extensive tables of the $B^{(s)}_{(c)}(R)$ coefficients, with (s) being short for $v_1, j_1, v_2, j_2, v_1', j_1', v_2', j_2'$ (results not shown). Note that for $v_1 \neq v_2$ we arbitrarily fix the phase factor of the matrix elements $\langle vj|r^n|v'j'\rangle$ so that $\langle 00|r|10\rangle$ is positive.

In order to reduce the volume of data to be reported, we describe the dependence on the rotational states (j_1, j_1', j_2, j_2') by a series expansion in terms of $j_i(j_i+1)$, etc., as it is common in molecular spectroscopy (Dunham expansion), according to

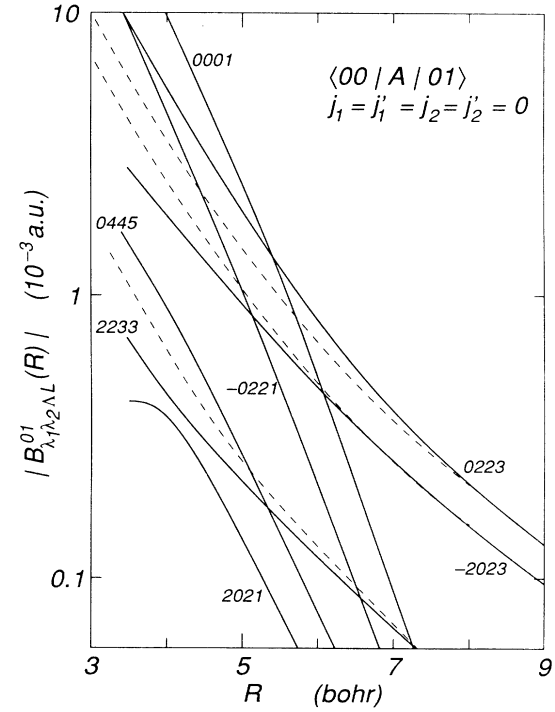

FIG. 1. Significant induced-dipole transition elements of H_2-H_2 pairs for the fundamental band (solid curves), for nonrotating molecules. The labels specified are the expansion parameter sets $\lambda_1\lambda_2\Lambda L$; a minus sign indicates negative B values. The dashed curves describe the long-range, quadrupole-induced contributions without overlap, Eq. (11).

TABLE III. Dipole moment expansion coefficients, $B_{\lambda_1,\lambda_2,\Lambda,L}(R)$, for the rototranslational band, in 10^{-6} a.u.

R (bohr) \ $\lambda_1\lambda_2\Lambda L$	0001	2023	0223	2021	0221	2233	2211	4045	0445	2245	2243	2223	2221	2201
						$A(r_0,r_0)$								
3.5	0	32 863	−32 863	−21 315	21 315	−3073	−670	2492	−2492	0	0	0	0	0
4.0	0	19 967	−19 967	−10 401	10 401	−1992	−332	1523	−1523	0	0	0	0	0
4.5	0	12 382	−12 382	−4850	4850	−1353	−160	842	−842	0	0	0	0	0
5.0	0	7953	−7953	−2190	2190	−949	−74	450	−450	0	0	0	0	0
5.5	0	5318	−5318	−974	974	−681	−34	243	−243	0	0	0	0	0
6.0	0	3688	−3688	−429	429	−498	−14	135	−135	0	0	0	0	0
7.0	0	1939	−1939	−84	84	−280	−2	47	−47	0	0	0	0	0
8.0	0	1119	−1119	−20	20	−166	0	19	−19	0	0	0	0	0
9.0	0	692	−692	−7	7	−104	0	9	−9	0	0	0	0	0
						$\langle 00\vert A\vert 00\rangle$								
3.5	0	33 581	−33 581	−22 244	22 244	−3124	−686	2726	−2726	0	0	0	0	0
4.0	0	20 378	−20 378	−10 911	10 911	−2025	−343	1678	−1678	0	0	0	0	0
4.5	0	12 605	−12 605	−5114	5114	−1376	−167	929	−929	0	0	0	0	0
5.0	0	8073	−8073	−2322	2322	−966	−78	495	−495	0	0	0	0	0
5.5	0	5385	−5385	−1039	1039	−694	−35	266	−266	0	0	0	0	0
6.0	0	3727	−3727	−461	461	−508	−15	148	−148	0	0	0	0	0
7.0	0	1954	−1954	−92	92	−286	−2	51	−51	0	0	0	0	0
8.0	0	1126	−1126	−22	22	−170	0	21	−21	0	0	0	0	0
9.0	0	696	−696	−7	7	−107	0	10	−10	0	0	0	0	0
						$\langle \bar{0}0\vert A\vert 00\rangle$								
3.5	59.4	29.6	−8.7	−27.8	1.5	−2.2	−0.5	4.7	0.2	−0.8	0.5	0	0.2	0.2
4.0	30.6	17.2	−6.2	−14.1	1.3	−1.4	−0.3	2.9	−0.1	−0.5	0.5	0	0.1	0.1
4.5	15.4	10.0	−4.3	−6.8	0.8	−1.0	−0.1	1.6	−0.2	−0.3	0.4	0.1	0	0.1
5.0	7.5	6.0	−3.0	−3.2	0.5	−0.7	−0.1	0.8	−0.1	−0.2	0.3	0.1	0	0
5.5	3.6	3.8	−2.1	−1.5	0.2	−0.5	0	0.4	−0.1	−0.1	0.2	0	0	0
6.0	1.6	2.5	−1.5	−0.7	0.1	−0.4	0	0.2	−0.1	−0.1	0.2	0	0	0
7.0	0.3	1.2	−0.8	−0.1	0	−0.2	0	0.1	0	0	0.1	0	0	0
8.0	0	0.7	−0.5	0	0	−0.1	0	0	0	0	0.1	0	0	0
9.0	0	0.4	−0.3	0	0	−0.1	0	0	0	0	0	0	0	0

TABLE IV. Dipole moment expansion coefficients $B_{\lambda_1,\lambda_2,\Lambda,L}(R)$ for the fundamental band, in 10^{-6} a.u.

R (bohr) \ $\lambda_1\lambda_2\Lambda L$	0001	2023	0223	2021	0221	2233	2211	4045	0445	2245	2243	2223	2221	2201
						$\langle 00\|A\|01\rangle$								
3.5	−18497	2648	−9236	−433	8776	−686	−165	−77	−1493	251	−149	−6	−53	−78
4.0	−9527	1883	−5366	−392	4441	−443	−87	42	−925	156	−152	−11	−27	−46
4.5	−4805	1313	−3113	−250	2145	−302	−45	55	−502	103	−130	−17	−10	−21
5.0	−2359	920	−1867	−139	1006	−214	−22	40	−260	66	−101	−17	−3	−9
5.5	−1118	655	−1175	−75	465	−156	−11	26	−135	41	−76	−14	0	−4
6.0	−511	474	−776	−40	212	−115	−5	17	−73	26	−56	−11	0	−1
7.0	−91	260	−382	−12	43	−66	−1	7	−24	11	−32	−6	1	0
8.0	−10	151	−214	−4	10	−39	0	3	−10	5	−19	−4	0	0
9.0	3	93	−131	−2	3	−25	0	1	−5	2	−12	−2	0	0
						$\langle 0\bar{0}\|A\|01\rangle$								
3.5	−27.4	108.9	−120.7	−70.2	86.2	−10.8	−2.4	8.4	−11.9	0.6	−0.2	0	−0.1	−0.2
4.0	−14.4	66.5	−72.7	−34.7	42.7	−7.0	−1.2	5.3	−7.3	0.4	−0.3	0	−0.1	−0.1
4.5	−7.4	41.3	−44.5	−16.4	20.2	−4.7	−0.6	3.0	−4.0	0.3	−0.3	0	0	−0.1
5.0	−3.8	26.6	−28.2	−7.5	9.3	−3.3	−0.3	1.6	−2.1	0.2	−0.2	0	0	0
5.5	−1.9	17.8	−18.6	−3.4	4.2	−2.4	−0.1	0.9	−1.1	0.1	−0.2	0	0	0
6.0	−0.9	12.4	−12.8	−1.5	1.9	−1.8	−0.1	0.5	−0.6	0.1	−0.1	0	0	0
7.0	−0.2	6.5	−6.6	−0.3	0.4	−1.0	−0	0.2	−0.2	0	−0.1	0	0	0
8.0	0	3.7	−3.8	−0.1	0.1	−0.6	0	0.1	−0.1	0	0	0	0	0
9.0	0	2.3	−2.4	0	0	−0.4	0	0	0	0	0	0	0	0
						$\langle 00\|A\|0\bar{1}\rangle$								
3.5	3.4	−108.4	107.6	71.5	−69.5	10.2	2.2	−8.8	7.9	0.2	0	0	0	0
4.0	1.5	−65.8	65.4	35.1	−33.9	6.6	1.1	−5.4	4.8	0.1	0	0	0	0
4.5	0.6	−40.7	40.6	16.5	−15.8	4.5	0.5	−3.0	2.7	0.1	0	0	0	0
5.0	0.2	−26.1	26.1	7.5	−7.1	3.1	0.3	−1.6	1.4	0.1	0	0	0	0
5.5	0	−17.4	17.5	3.3	−3.2	2.3	0.1	−0.9	0.8	0	0	0	0	0
6.0	0	−12.1	12.1	1.5	−1.4	1.7	0	−0.5	0.4	0	0	0	0	0
7.0	0	−6.3	6.4	0.3	−0.3	0.9	0	−0.2	0.2	0	0	0	0	0
8.0	0	−3.6	3.7	0.1	−0.1	0.6	0	−0.1	0.1	0	0	0	0	0
9.0	0	−2.3	2.3	0	0	0.3	0	0	0	0	0	0	0	0

$$B^{(s)}_{(c)}(R)\approx\langle v_1 0 v_2 0|A_{(c)}|v_1' 0 v_2' 0\rangle+\langle \overline{v_1} v_2|A_{(c)}|v_1' v_2'\rangle j_1(j_1+1)+\langle v_1\overline{v_2}|A_{(c)}|v_1' v_2'\rangle j_2(j_2+1)$$
$$+\langle v_1 v_2|A_{(c)}|\overline{v_1'} v_2'\rangle j_1'(j_1'+1)+\langle v_1 v_2|A_{(c)}|v_1'\overline{v_2'}\rangle j_2'(j_2'+1)+\cdots \quad (7)$$

for the two cases $v_1=v_2=0$ and $v_1'=0$, $v_2'=1$. The leading coefficients in this expansion are the components $B^{v_1 v_1' v_2 v_2'}_{(c)}(R)$ that correspond to nonrotating molecules ($j_1=j_1'=j_2=j_2'=0$). The remaining terms are corrections that account for the rotational dependences. The case of molecule 1 undergoing a vibrational transition ($v_1'=1$, $v_2'=0$) is readily obtained from this by making use of the symmetry relations

$$\langle 00|A_{\lambda_1\lambda_2\Lambda L}|01\rangle=(-1)^{\Lambda-L}\langle 00|A_{\lambda_2\lambda_1\Lambda L}|10\rangle\ , \quad (8)$$

$$\langle v_1 j_1 v_2 j_2|A_{\lambda_1\lambda_2\Lambda L}|v_1' j_1' v_2' j_2'\rangle$$
$$=(-1)^{\Lambda-L}\langle v_2 j_2 v_1 j_1|A_{\lambda_2\lambda_1\Lambda L}|v_2' j_2' v_1' j_1'\rangle\ . \quad (9)$$

For the range of j values of interest here, we found that higher than linear terms can safely be neglected, just as this was seen in related work on the H_2-He system.[24] The nonredundant coefficients for the RT band are listed in Table III and those of the fundamental RV band of H_2 in Table IV for various separations R. Coefficients not listed are either negligible, e.g., $\langle\overline{00}|A|01\rangle$, or related to one of the coefficients given by the relation, Eq. (9).

The most significant induced-dipole components are shown in Fig. 1 as function of separation R for the case of nonrotating molecules ($j_1=j_1'=j_2=j_2'=0$). Just as this was seen previously for gas mixtures like H_2-He, the nearly exponential isotropic overlap component ($\lambda_1\lambda_2\Lambda L=0001$) dominates at small R, and the quadrupole-induced components, 0223 and 2023, are most significant at large R. The dashed lines correspond to the classical, pure quadrupole induction term (with the overlap contribution suppressed), see Eqs. (11) below. These reflect the characteristic R^{-4} dependence. Apart from the fact that some of the pairs, like 0221,2021 that are identical in the rototranslational band, differ distinctly in the fundamental band on account of the vibrational excitation of *one* molecule, the picture looks very similar to the ones shown previously. We note that the signs of the B components indicated in the figure (i.e., the sign attached to some labels, as in -0221) correspond to molecule 2 undergoing the vibrational transition. According to Eq. (8), another identical set of $|B|$ coefficients exists that corresponds to molecule 1 undergoing the vibrational transition.

It is easy to see that the use of the induced-dipole components of nonrotating molecules, Fig. 1, in line-shape calculations results in poor agreement with the measurements. Specifically, the computed $S_1(j)$ line profiles would be too intense, especially for large j, and similar inconsistencies would be noticeable in the $O_1(j)$ lines. For the vibrational bands, these j dependences must be taken into account. We give, therefore, $j(j+1)$ expansion coefficients in the lower part of Table IV which, when used as in Eq. (7) will modify the data shown in Fig. 1 and in the upper part of Table IV. With these, at least for the smaller j values ($0\le j\le 3$), the actual j dependence is closely modeled, Eq. (7).

Table IV shows that several of these correction coefficients are of nearly the same magnitude but of opposite sign, for example, for the $\lambda_1\lambda_2\Lambda L=2023$ and 0223 components, $\langle 0\overline{0}|A|01\rangle$ and $\langle 00|A|0\overline{1}\rangle$. Therefore, in Fig. 2 we need to give only one representative example of these functions. A similar situation exists for the four correction terms of the 2021,2021 components. The comparison of Figs. 1 and 2 shows that the correction terms belonging to the same $\lambda_1\lambda_2\Lambda L$ set show very much the same dependence as the dipole coefficient for the rotationless case, i.e., the quadrupole-induced terms reflect the R^{-4} dependence and the overlap terms are scaled-down versions of exponential functions similar to the ones shown in Fig. 1. In other words, the $j_1'j_2'$ corrections amount more or less to a *scaling* of the B coefficients. This fact, in turn, has the consequence that the spectral profiles associated with a certain $\lambda_1\lambda_2\Lambda L$ are, to a first approximation, simply scaled by a factor that depends on the rotational quantum numbers involved;

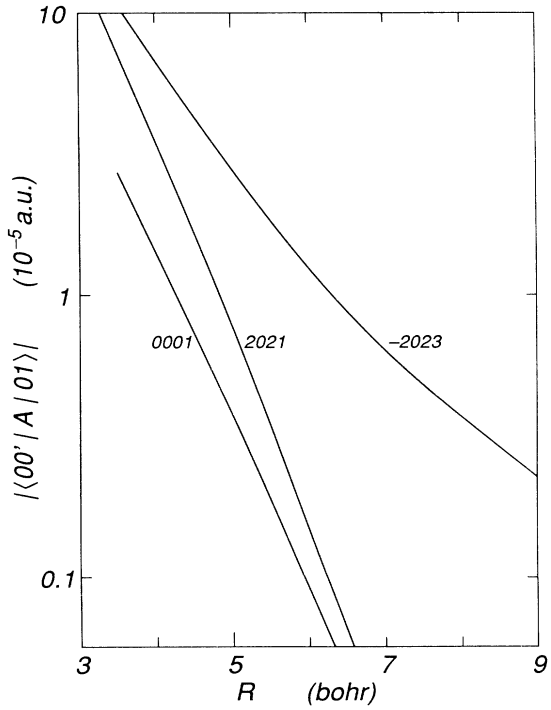

FIG. 2. Selected coefficients $\langle 0\overline{0}|A|01\rangle$ to correct the transition elements $\langle 00|A|01\rangle$ for rotation of the molecules, see Eq. (7) for definition.

whereas the *line shape* is not very strongly j dependent, the *line intensities* are.

For the calculation of spectral profiles an analytical form of the expansion coefficients $B^{(s)}_{(c)}(R)$, Eq. (7), is desirable. The numerical results of Tables III and IV are described quite accurately by functions of the form

$$B_{(c)}(R)=\frac{B^{(n)}_{(c)}}{R^n}+B^{(0)}_{(c)}\exp[a_c(R-R_0)+b_c(R-R_0)^2] , \tag{10}$$

where the subscript c is short for $\lambda_1\lambda_2\Lambda L$. Equation (10) is a slight generalization of a similar form in general use.[21,45] The parameter $R_0=6$ bohr has been chosen to be close to the collision diameter so that $B^{(0)}_{(c)}$ gives the approximate size of the exchange and distortion dipole contribution at the collision diameter. The $B^{(n)}_{(c)}$ account for the long-range induction or dispersion contributions, with an n value appropriate for the leading term [see Eq. (11) below]. It should be noted that the parameter $B^{(n)}_{(c)}$ comprises small contributions from higher-order terms that are effective at the distances from 7 to 9 bohrs, while the damping of the long-range terms, which is relatively large only for the weak dispersion term, is absorbed in the second term of Eq. (10). The parameters of the fit are collected in Tables V and VI. Since intermolecular separations of 3.5 bohr are not significant for the computation of the spectra, we have excluded this distance from the fit. For the remaining eight distances, the four-parameter analytical fit, Eq. (10), reproduces the input data of Tables III and IV to better than 0.5% for the three leading components, and to better than 3% for the remaining small ones.

Asymptotically, the induced-dipole components are determined by the multipole moments and polarizability invariants of H_2. A general expression and the three leading terms have been given in an appendix of Ref. 18. If we write briefly $|i\rangle$ for $|v_i j_i\rangle$, we have

$$\begin{aligned}
&B^{(s)}_{2023}(R)\to\sqrt{3}\langle 1|\alpha|1'\rangle\langle 2|q_2|2'\rangle/R^4 ,\\
&B^{(s)}_{0223}(R)\to-\sqrt{3}\langle 2|\alpha|2'\rangle\langle 1|q_2|1'\rangle/R^4 ,\\
&B^{(s)}_{2233}(R)\to\sqrt{2/15}(\langle 1|\gamma|1'\rangle\langle 2|q_2|2'\rangle\\
&\qquad\qquad+\langle 2|\gamma|2'\rangle\langle 1|q_2|1'\rangle)/R^4 ,\\
&B^{(s)}_{4045}(R)\to\sqrt{5}\langle 1|\alpha|1'\rangle\langle 2|q_4|2'\rangle/R^6 ,\\
&B^{(s)}_{0445}(R)\to-\sqrt{5}\langle 2|\alpha|2'\rangle\langle 1|q_4|1'\rangle/R^6 .
\end{aligned} \tag{11}$$

TABLE V. Fit parameters for the rototranslational band, in 10^{-6} a.u.; numbers in square brackets designate powers of 10.

$\lambda_1\lambda_2\Lambda L$	n	$B^{(n)}$	$B^{(0)}$	a	b
			$A(r_0r_0)$		
2023	4	0.453[+1]	0.190[−3]	−1.332	−0.041
0223	4	−0.453[+1]	−0.190[−3]	−1.332	−0.041
2021	7	−0.274[+2]	−0.331[−3]	−1.797	−0.079
0221	7	0.274[+2]	0.331[−3]	−1.797	−0.079
2233	4	−0.687[+0]	0.313[−4]	−1.576	−0.015
2211	7	0.150[+1]	−0.197[−4]	−1.587	−0.027
4045	6	0.442[+1]	0.399[−4]	−1.655	−0.216
0445	6	−0.442[+1]	−0.399[−4]	−1.655	−0.216
			$\langle 00\|A\|00\rangle$		
2023	4	0.456[+1]	0.209[−3]	−1.346	−0.040
0223	4	−0.456[+1]	−0.209[−3]	−1.346	−0.040
2021	7	−0.312[+2]	−0.348[−3]	−1.792	−0.082
0221	7	0.312[+2]	0.348[−3]	−1.792	−0.082
2233	4	−0.702[+0]	0.333[−4]	−1.566	−0.016
2211	7	0.182[+1]	−0.218[−4]	−1.561	−0.021
4045	6	0.462[+1]	0.514[−4]	−1.404	−0.090
0445	6	−0.462[+1]	−0.514[−4]	−1.404	−0.090
			$\langle\bar{0}0\|A\|00\rangle$		
0001	7	−0.250[+0]	0.252[−5]	−1.450	0.000
2023	4	0.279[−2]	0.361[−6]	−1.491	−0.028
0223	4	−0.210[−2]	0.768[−7]	−1.449	0.095
2021	0	0.0[+0]	−0.675[−6]	−1.581	−0.034
0221	0	0.0[+0]	0.128[−6]	−1.387	−0.106
2233	4	−0.529[−3]	0.357[−7]	−1.464	−0.014
2211	0	0.0 [+0]	−0.179[−7]	−1.452	−0.037
4045	6	0.720[−2]	0.431[−7]	−2.897	−0.683
0445	6	−0.280[−2]	−0.290[−8]	−2.795	−0.094

In these expressions, the $\langle i|\alpha|i'\rangle$, $\langle i|\gamma|i'\rangle$, and $\langle i|q_\lambda|i'\rangle$ are the radial matrix elements of trace and anisotropy of the H_2 polarizability tensor and the multipole moment of order λ, respectively. We note that both sides of Eq. (11) can be expanded in power series of $j(j+1)$, just as was done in Eq. (7). The expansion coefficients thus obtained from accurate values of polarizabilities and quadrupole moments[37,46–48] are included in Table I and compared with the $B^{(n)}$ obtained from the fits of the induced-dipole curves according to Eq. (10). In our previous work on the rototranslational band,[18] the long-range coefficients obtained from calculations at the single bond distance $r_0=1.449a_0$ were shown to be in close agreement with accurate values from Eq. (11). Table I verifies that this holds also for the vibrational transition matrix elements relevant for the fundamental band, including their rotational dependence. The somewhat larger deviations involving the small components due to the hexadecapole moment can be traced to the difficulties to separate the long-range part from the overlap contributions in a least-squares fit.

The very satisfying agreement between the long-range coefficients $B_c^{(n)}$ of the leading components with their accurate asymptotic values demonstrates that our CI wave function separates correctly for large internuclear distances. From this agreement and the degree to which the induction contributions are dominant over all distances, we assess the accuracy of the *ab initio* calculated dipole moments to be in the order of 3%.

III. POTENTIAL

In order to compute a spectral profile, a potential function must be used that models the interaction closely, especially in the region near the collision diameter that is so important for CIA spectra. The interaction of hydrogen molecules has been a subject of intense research,[49] but no potential has been available which is applicable to vibrationally excited hydrogen. Since our previous work on H_2-He has demonstrated the significance of potential differences in entrance and exit channels of the spectroscopic transitions, a new attempt was made to determine the vibrationally averaged isotropic potential from *ab initio* calculations. This new potential, which will be described in detail elsewhere,[50] is a significant improvement over previous *ab initio* potentials. However, com-

TABLE VI. Fit parameters for the rotovibrational band, in 10^{-6} a.u.; numbers in square brackets designate powers of 10.

$\lambda_1\lambda_2\Lambda L$	n	$B^{(n)}$	$B^{(0)}$	a	b
			$\langle 00\|A\|01\rangle$		
0001	7	0.382[+2]	−0.652[−3]	−1.521	−0.033
2023	4	0.622[+0]	−0.811[−5]	−2.268	−0.074
0223	4	−0.853[+0]	−0.118[−3]	−1.479	−0.026
2021	7	−0.155[+2]	0.148[−4]	−1.219	0.283
0221	7	0.161[+2]	0.153[−3]	−1.806	−0.130
2233	4	−0.163[+0]	0.107[−4]	−1.507	−0.028
2211	7	0.105[+1]	−0.862[−5]	−1.431	−0.002
4045	6	0.779[+0]	−0.316[−6]	−3.755	−0.341
0445	6	−0.220[+1]	−0.295[−4]	−1.430	−0.131
			$\langle 0\bar{0}\|A\|01\rangle$		
0001	0	0.0	−0.883[−6]	−1.517	−0.063
2023	4	0.152[−1]	0.645[−6]	−1.307	−0.044
0223	4	−0.154[−1]	−0.883[−6]	−1.402	−0.035
2021	0	0.0	−0.152[−5]	−1.597	−0.014
0221	0	0.0	0.190[−5]	−1.598	−0.018
2233	4	−0.244[−2]	0.122[−6]	−1.557	−0.019
2211	0	0.0	−0.572[−7]	−1.665	−0.070
4045	6	−0.176[−1]	−0.106[−6]	−1.884	−0.372
0445	6	0.195[−1]	0.200[−6]	−1.688	−0.196
			$\langle 00\|A\|0\bar{1}\rangle$		
0001	7	−0.161[−1]	0.318[−7]	−2.657	−0.232
2023	4	−0.148[−1]	−0.667[−6]	−1.339	−0.036
0223	4	0.149[−1]	0.616[−6]	−1.311	−0.036
2021	0	0.0	0.150[−5]	−1.617	−0.017
0221	0	0.0	−0.141[−5]	−1.629	−0.017
2233	4	0.228[−2]	−0.105[−6]	−1.576	−0.016
2211	7	−0.534[−2]	0.679[−7]	−1.569	−0.022
4045	6	−0.176[−1]	−0.990[−7]	−1.910	−0.332
0445	6	0.170[−1]	0.602[−7]	−2.277	−0.497

TABLE VII. The interaction potential, in 10^{-6} hartree.

R (bohr)	$\langle 00\|V\|00\rangle$[a]	$\langle 00\|V\|00\rangle$[b]	$\langle 01\|V\|01\rangle$[b]	$\langle 11\|V\|11\rangle$[b]	$\langle 02\|V\|02\rangle$[b]
3.5	17 883.3	18 872.3	19 425.3	19 965.5	19 978.8
4.0	7117.0	7608.6	7925.3	8238.5	8252.8
4.5	2518.6	2810.5	2972.8	3135.0	3144.6
5.0	771.5	880.2	952.2	1024.6	1030.1
5.5	125.4	166.7	192.7	218.9	221.7
6.0	−73.4	−60.2	−54.7	−49.3	−47.9
6.5	−111.6	−107.7	−109.9	−112.4	−111.8
7.0	−98.7	−98.1	−102.3	−106.8	−106.5
8.5	−39.2	−39.3	−41.7	−44.3	−44.3
10.0	−14.5	−14.5	−15.4	−16.3	−16.3

[a]From Ref. 51.
[b]Present results (Ref. 50).

parison of measured and calculated virial coefficients indicates that the dispersion attraction still falls short by about 2%. For the present purpose we have, therefore, chosen a potential for nonvibrating H_2 pairs which has been developed by Schäfer[51] by adjusting Meyer's earlier anisotropic *ab initio* potential[25,52] to reproduce the measured virial data from theory. This semiempirical potential has been shown to also reproduce a number of discriminating measurements[53–55] and may be considered the most reliable potential surface presently available.

For the sake of a complete documentation, the first column of Table VII repeats the semiempirical model.[51] The remaining columns of the table are new *ab initio* results. Specifically, the second column gives the vibrational average of nonvibrating molecules, $v_1=v_2=0$ of the isotropic part obtained by a recent, extended computation.[50] The third column specifies similarly the vibrational average when one molecule is excited, $v_1=0$, $v_2=1$. Such an average is needed to describe the final state. Since the data in columns 2 and 3 are not quite as refined as those of column 1, we compute an improved model of the interaction for the case of a vibrationally excited H_2 by adding to column 1 the differences of columns 3 and 2 at each fixed R,

$$\Delta_{v_1v_2}V_0(R)=\langle v_1v_2|V_0(R;r_1r_2)|v_1v_2\rangle - \langle 00|V_0(R;r_1r_2)|00\rangle , \quad (12)$$

for $v_1=0$ and $v_2=1$.

In Table VII, we also specify vibrational elements of the *ab initio* potential surface for the case of two excited molecules $v_1=v_2=1$ (fourth column), and for the case of a doubly excited H_2 ($v_1=0$, $v_2=2$, column 5) that will be used similarly in future work concerned with the first overtone CIA spectra.

IV. LINE-SHAPE THEORY

In the fundamental band, the absorption coefficient at the angular frequency $\omega=2\pi c\nu$ arising from collision-induced dipoles in molecular pairs can be written as[1,2]

$$\alpha(\omega;T)=\frac{2\pi^2}{3\hbar c}n^2\omega Vg(\omega;T) , \quad (13)$$

where n is the number density of the gas, V is the volume, and T is the temperature. The density ρ is usually expressed in units of amagat, in which case n is equal to ρN_A, $N_A=2.686\,76\times10^{19}$ cm^{-3}amagat^{-1} being Loschmidt's number. The spectral density $g(\omega;T)$ is defined in terms of the matrix elements of the induced electric dipole moment μ by the "golden rule,"

$$g(\omega;T)=\sum_{s,s'}P_s\sum_{t,t'}P_t|\langle t|\mu_{ss'}|t'\rangle|^2\delta(\omega_{ss'}+\omega_{tt'}-\omega) . \quad (14)$$

The subscripts $s=\{j_1,m_1,v_1,j_2,m_2,v_2\}$ and $t=\{l,m_l,E_t\}$ denote molecular and translational states, respectively; the j,m refer to rotational states and the v to vibrational states of H_2, the subscripts 1 and 2 refer to molecules 1 and 2, and a prime denotes final states. The normalized translational Boltzmann factor is given by

$$P_t(T)=\frac{\lambda_0^3}{V}e^{-E_t/kT}, \quad \lambda_0=\left[\frac{2\pi\hbar^2}{mkT}\right]^{1/2} \quad (15)$$

where λ_0 is the thermal de Broglie wavelength. The rotational Boltzmann factor is written as $P_s(T)=P_{j1}(T)P_{j2}(T)$, with

$$P_j(T)=\frac{g_j\exp(-E_j/kT)}{\sum_J g_J(2J+1)\exp(-E_J/kT)} . \quad (16)$$

The nuclear weights of hydrogen are $g_j=1$ for even j, and $g_j=3$ for odd j.

We mention that in low-temperature laboratory measurements as well as in astrophysical applications, para-H_2 and ortho-H_2 abundances may differ from the proportions characteristic for thermal equilibrium [Eq. (16)]. In such case, at any fixed temperature T, one may formally account for nonequilibrium proportions by assuming g_j values so that the ratio g_0/g_1 reflects the actual para-to-ortho abundance ratio.

We note that the separability of the translational states from the rotovibrational states requires that the potential be isotropic. For H_2, this is nearly true. Although the

potential function has appreciable anisotropic terms, the rather large rotational quanta of H_2 ensure the neglect of these terms to be a good approximation, which we will use throughout the work. We note, furthermore, that the product $Vg(\omega;T)$ actually does not depend on V because of the reciprocal V dependence of P_t, Eq. (15).

We obtain the spectral function as a multiple sum of incoherent components,[56]

$$g(\omega;T)=\sum_{\lambda_1,\lambda_2,\Lambda,L}\sum_{j_1,j_1',j_2,j_2'}(2j_1+1)P_{j_1}[C(j_1\lambda_1 j_1';000)]^2(2j_2+1)P_{j_2}[C(j_2\lambda_2 j_2';000)]^2 \times G^{j_1 j_1' j_2 j_2'}_{\lambda_1\lambda_2\Lambda L}(\omega-\omega_{j_1 v_1 j_1' v_1'}-\omega_{j_2 v_2 j_2' v_2'};T) \ . \tag{17}$$

In the isotropic potential approximation, the complete spectrum is obtained by superimposing basic line profiles, which we will refer to as translational components, $G^{j_1 j_1' j_2 j_2'}_{\lambda_1\lambda_2\Lambda L}(\bar{\omega};T)$; the $\bar{\omega}$ designate frequency shifts relative to the line centers which are sums of molecular rotovibrational frequencies, $\omega_{j_1 v_1 j_1' v_1'}$ and $\omega_{j_2 v_2 j_2' v_2'}$; the latter may be positive, zero and negative. The translational profiles are given by

$$\begin{aligned}VG^{(s)}_{(c)}(\bar{\omega};T)=\lambda_0^3\hbar\sum_{l,l'}(2l+1)[C(lLl';000)]^2[1+(-1)^l\gamma_S] \\ \times\Bigg[\int_0^\infty\exp\left(-\frac{E_t}{kT}\right)dE_t|\langle l,E_t,v|B^{(s)}_{(c)}(R)|l',E_t+\hbar\bar{\omega},v'\rangle|^2 \\ +\sum_{n,n'}\exp\left(-\frac{E_{nl}}{kT}\right)|\langle l,E_{nl},v|B^{(s)}_{(c)}(R)|l',E_{n'l'},v'\rangle|^2\delta(\Delta_{nln'l'}-\hbar\bar{\omega}) \\ +\sum_{n}\exp\left(-\frac{E_{nl}}{kT}\right)|\langle l,E_{nl},v|B^{(s)}_{(c)}(R)|l',E_{nl}+\hbar\bar{\omega},v'\rangle|^2 \\ +\sum_{n'}\exp\left(-\frac{E_{n'l'}-\hbar\bar{\omega}}{kT}\right)|\langle l,E_{n'l'}-\hbar\bar{\omega},v|B^{(s)}_{(c)}(R)|l',E_{n'l'},v'\rangle|^2\Bigg] \ .\end{aligned} \tag{18}$$

In this expression, $\Delta_{nln'l'}=E_{n'l'}-E_{nl}$ and the terms in brackets $\langle\cdots\rangle$ represent radial matrix elements,

$$\langle l,E,v|B^{(s)}_{(c)}|l',E',v'\rangle = \int_0^\infty\psi^*(R;l',E',v')B^{(s)}_{(c)}(R)\psi(R;l,E,v)dR \ , \tag{19}$$

with vibration-dependent functions ψ defined below. The constant γ_S accounts for the molecular interchange symmetry.[18] For the low-resolution CIA RV spectra, we find that exchange symmetry only matters at temperatures much lower than 20 K; only the generally weak dimer structures are discernibly affected by symmetry. At temperatures above 20 K, one may simply set $\gamma_S=0$.

The expression to the right of Eq. (18) consists of a sum of four terms. The first one, the integral, represents the free→free transitions of the collisional pair and is usually the dominant term. The second term, a sum, gives the bound→bound transitions of the van der Waals dimers. The vibrational and rotational quantum numbers of the dimer are designed by n and l; l also numbers the partial waves. For practical purposes, one will convolute the δ function with some suitable instrumental or line profile for a more realistic simulation of the observation. The remaining two terms account for bound→free and free→bound transitions of the molecular pair, respectively. We note that the energies $E_{nl}+\hbar\omega$ and $E_{n'l'}-\hbar\omega$ appearing in these terms must be legitimate free state energies, i.e., they must be positive or else the radial matrix elements vanish.

We note that the computational effort to derive the various j,j'-dependent profiles G is considerably reduced by making use of the Dunham approximation, Eq. (7). Inserting Eq. (7) into Eq. (18) yields a similar $j(j+1)$ expansion for G. Since two of the five terms listed in Tables V and VI are negligibly small, only three radial integrals $\langle l,E,v|B|l',E+\hbar\omega,v'\rangle$ are really required to account for the rotational dependencies up to linear terms in $j(j+1)$ which is a very good approximation for the j values needed here.

The radial wave functions $\psi(R;l,E_t,v)/R$ needed for the computation of Eq. (18) are solutions of the Schrödinger equation of relative motion of the molecular pair,

$$-\frac{\hbar^2}{2m}\frac{d^2\psi}{dR^2}+\left[V_0^v(R)+\frac{\hbar^2 l(l+1)}{2mR^2}-E_t\right]\psi=0 \ , \tag{20}$$

where v is short for the vibrational state v_1v_2 of the H_2-H_2 pair and

$$V_0^v(R)=\langle v_1v_2|V_0(R;r_1,r_2)|v_1v_2\rangle \ , \tag{21}$$

where $V_0(R;r_1,r_2)$ is the interaction potential which de-

pends on the vibrational coordinates. The weak j_1, j_2 dependence of the potential is suppressed, but the much stronger dependence on the vibrational excitation cannot be ignored. For easy integration of Eq. (18), free-state wave functions are energy normalized,

$$\int_0^\infty \psi^*(R;l,E_{t'},v)\psi(R;l,E_t,v)dR = \delta(E_{t'}-E_t) , \quad (22)$$

for any fixed l. For bound states, the δ function in Eq. (22) is replaced by the Kronecker delta symbol, $\delta_{nn'}$, as usual; E_t is then replaced by E_{nl}, which is negative. (It is also v_1, v_2 dependent.)

The spectral function, Eq. (17), consists of a number of lines at rotovibrational transition frequencies of H_2 and lines at sums and differences of such rotation frequencies. Most prominent are the S and Q lines corresponding to $j \to j+2$ and $j \to j$, respectively. The Clebsch-Gordan coefficients in Eqs. (17) and (18) indicate selection rules $|j_i - \lambda_i| \le j_i' \le j_i + \lambda_i$, and $|l-L| \le l' \le l+L$. Furthermore, $j_i + j_i' \ge \lambda_i$ for $i=1,2$ and $l+l' \ge L$.

Translational moments are often quoted in experimental work and hence are here of interest. These are integrals of Eq. (18) over frequency shift $\bar{\omega}$,

$$M_n(T;\lambda_1\lambda_2\Lambda L) = \int_{-\infty}^{\infty} VG_{\lambda_1\lambda_2\Lambda L}(\bar{\omega};T)\bar{\omega}^n d\bar{\omega} . \quad (23)$$

For $n=0,1,2$, these moments can be also computed directly from the potential function and induction operator using well-known sum rules,[28] which fact offers a desirable test of the numerical precision attained in the line-shape calculations. Since hydrogen pairs at the temperatures of interest must be considered wave mechanical systems, an exact quantum formalism is used for our tests which is described elsewhere.[28,57]

Other moments (sometimes referred to as "spectral invariants") are often specified in experimental investigations are certain normalized integrals of the RV spectra over frequency,

$$\gamma_1 = \frac{\hbar}{2kT}\frac{1}{\rho^2}\int_0^\infty \alpha(\omega;T)\frac{d\omega}{\omega} , \quad (24)$$

$$\alpha_1 = \frac{1}{\rho^2}\int_0^\infty \alpha(\omega;T)d\omega . \quad (25)$$

These moments are functions of temperature that may be obtained from the spectra $\alpha(\omega;T)$.

V. RESULTS

For the significant $\lambda_1\lambda_2\Lambda L$ induction components, we have computed values of the various spectral functions at about twenty points, over a frequency band of up to ± 1800 cm^{-1} relative to the line center, and the temperatures from 20 to 300 K for which measurements exist. In related work we shall communicate analytical approximations of the computed spectral profiles at the temperatures between 40 and 300 K for easy modeling of radiative transfer in planetary atmospheres which permits the reproduction of the present line shape computational results in seconds.

The spectra of bound dimers, $(H_2)_2$, have been recorded in the fundamental bands.[1,58–60] However, as far as the low-resolution spectra of our current interest are concerned, dimer features are not readily discernible (albeit they are present); see, however, Fig. 10. Rather, free-bound transitions involving dimers contribute several

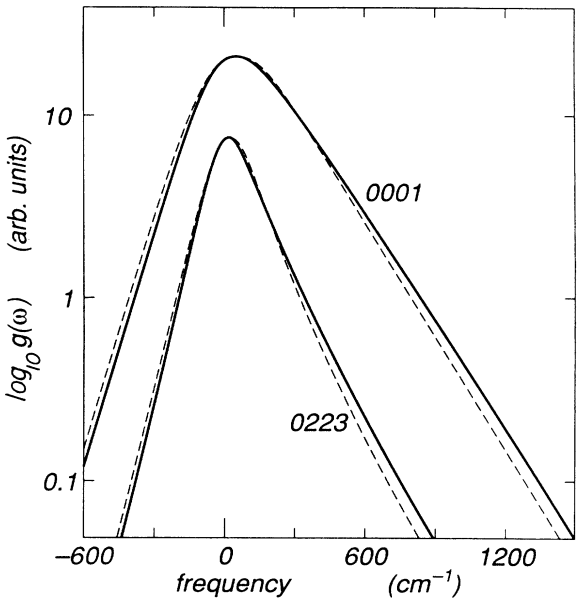

FIG. 3. Symmetry of the line profiles at 297 K. Top, isotropic overlap component ($\lambda_1\lambda_2\Lambda L=0001$); bottom, quadrupole-induced component ($\lambda_1\lambda_2\Lambda L=0223$); dashed curves, ditto, assuming, however, the same interaction potential for initial and final translational state of the pair.

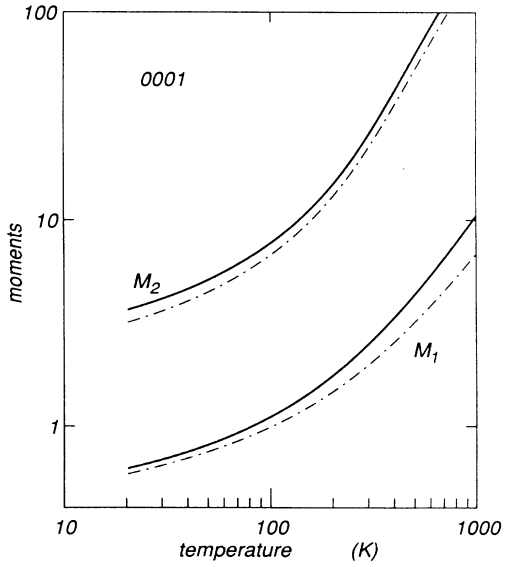

FIG. 4. First and second moments of the $\lambda_1\lambda_2\Lambda L=0001$ component as function of temperature; units of 1×10^{-50} erg cm^6/s for the first moment and 1×10^{-37} erg cm^6/s^2 for the second.

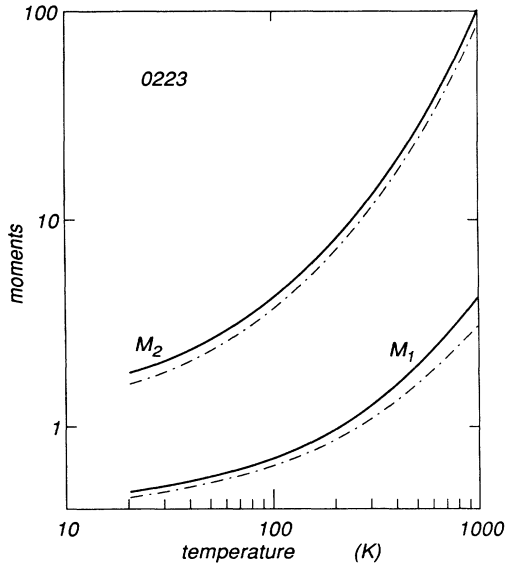

FIG. 5. First and second moments of the $\lambda_1\lambda_2\Lambda L=0223$ component as function of temperature; units of 1×10^{-50} erg cm^6/s for the first moment and 1×10^{-37} erg cm^6/s^2 for the second.

percent to the observable spectra in the form of relatively unstructured, broad continua near the $S_1(j)$, etc., line centers. While our theory is capable of modeling the major features involving dimers,[61,62] we refrain from an accurate modeling of the weak features that are discernible at high enough resolution; these are usually pressure broadened. We do, however, include the diffuse bound-free contributions.

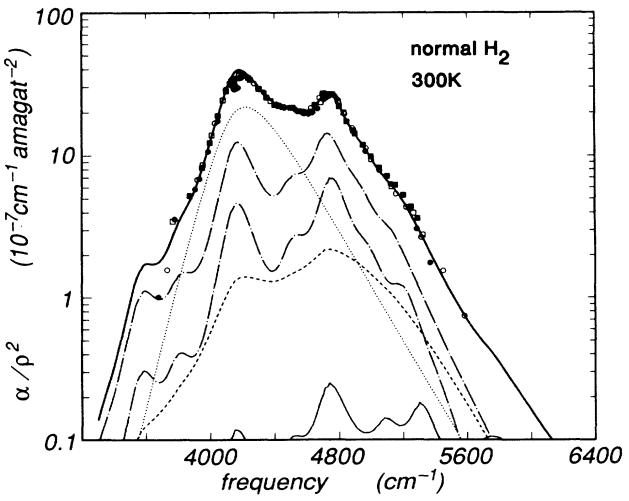

FIG. 6. Binary CIA spectrum at 300 K: calculated from first principles (heavy line). Measurements: dots from Ref. 70; circles from Ref. 71; squares from Ref. 72. Also shown are intermediate computational results, namely, the $\lambda_1\lambda_2\Lambda L$ components 0001 (dotted); 0223 and 2023 (dot-dashed); 0221 (dashes); 4045 and 0445 (short dash-long dash); and 2233 (thin solid line).

We note that a careful computational study of the dimer features is very involved. It must account for the anisotropy of the interaction as this was recently done for the pure rotational bands of hydrogen pairs.[19,63] Whereas our treatment may be expected to predict nearly correct main features and total intensities of the free-bound, bound-free, and bound-bound transitions involving the $(H_2)_2$ van der Waals molecule (and, of course, the free-free transitions which make up more than 90% of the observed intensities), the anisotropy of the interaction causes elaborate fine structure that is of considerable interest for the measurement of the anisotropy.[49]

Recent reviews[64] suggest that the effect of molecular vibrations has not been studied in RV CIA spectra of H_2 pairs due to the lack of a reliable interaction potential. We have provided above such data for hydrogen pairs and are, therefore, in a position to study the influence of molecular vibrations on the CIA spectra. Similar work on the H_2-He system indicated significant effects of vibration on the spectral moments and the symmetry of the lines.[23,27,28]

As an example, Fig. 3 compares the $\lambda_1\lambda_2\Lambda L=0001$ and 2023 line profiles at 300 K which were computed with and without (solid and dashed curves, respectively) accounting for the vibrational dependences of the interaction potential. The correct profiles (solid curves) are more intense in the "blue" wing, and less intense in the "red" wing by up to 25% relative to the approximation (dashed), over the range of frequencies shown. Whereas the dashed profiles satisfy the familiar "principle of detailed balance," Eq. (1), if ω is taken to mean the frequency shift ($\bar{\omega}$) relative to the line center, the exact profiles deviate by up to a factor of 2 from that equation over the range of frequencies shown. In a comparison of theory and measurement the different symmetries are quite striking; use of the correct symmetry substantially improves the quality of the fits attainable.

Whereas zeroth moments M_0 of the fundamental band profiles are not affected by the interaction of the final state of the collisional pair, all higher moments are, especially the odd moments at high temperatures. Figures 4 and 5 show first and second moments of the $\lambda_1\lambda_2\Lambda L=0001$ and 0223 profiles as function of temperature. For comparison, moments computed with the *same* interaction potential of initial and final states are also shown (dashed).

Figures 6–10 compare the computational results to the existing measurements. All measurements shown agree very closely with the fundamental theory except for the dips noticeable in the measured data near 4160 cm^{-1}, the "intercollisional dips."[65,66] That feature arises from correlations of the induced dipoles in subsequent collisions. It cannot be described by a theory that considers binary interactions only. Apart from that feature, the agreement at the higher temperatures, Figs. 6–8 is indeed a very close one. In the figures, we have chosen the dot size to suggest an uncertainty of ±3.5% relative to the center, or 7% end to end. In most cases, the agreement of theory and measurement is within that range. We note that no adjustable parameters were used anywhere in the

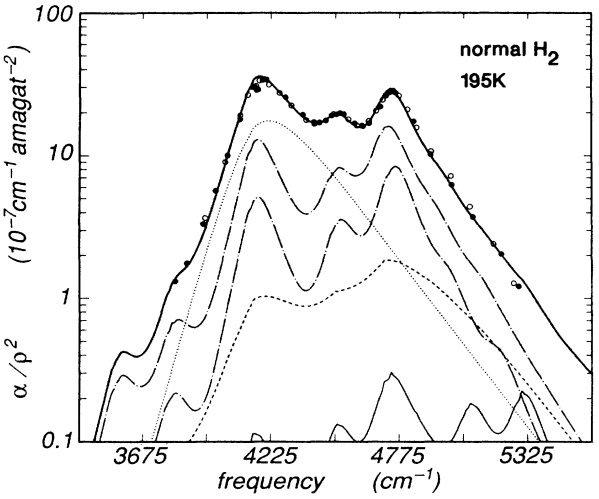

FIG. 7. Binary CIA spectrum at 195 K: calculated from first principles (heavy line). Measurements: dots from Ref. 70; circles from Ref. 71. Also shown are intermediate computational results, namely, the $\lambda_1\lambda_2\Lambda L$ components 0001 (dotted); 0223 and 2023 (dot-dashed); 0221 (dashes); 4045 and 0445 (short dash-long dash); and 2233 (thin solid line).

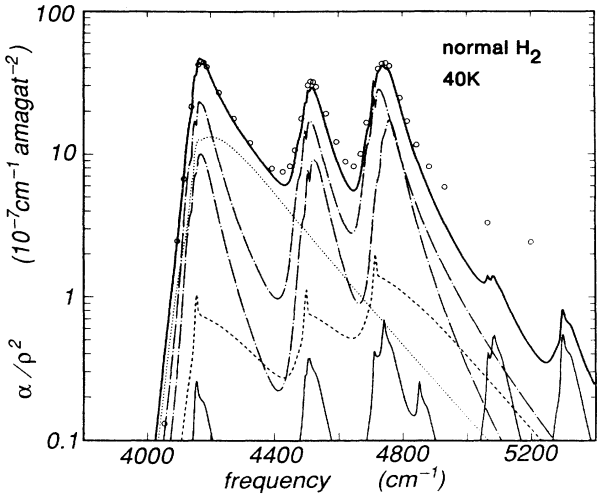

FIG. 9. Binary CIA spectrum at 40 K: calculated from first principles (heavy line). Measurements: circles from Ref. 72. Also shown are intermediate computational results, namely, the $\lambda_1\lambda_2\Lambda L$ components 0001 (dotted); 0223 and 2023 (dot-dashed); 0221 (dashes); 4045 and 0445 (short dash-long dash); and 2233 (thin solid line).

theory. Rather, the agreement is in terms of absolute intensities. At the lower temperatures, measured high-frequency wings appear more intense than the fundamental theory suggests. At 40 K, the differences are much greater than both at higher (77 K) and lower (20 K) temperatures; see Figs. 8–10. New measurements of the high-frequency wings at low temperatures are desirable to assess the possible significance of the inconsistencies observed at 40 K.

For the H_2-H_2 rototranslational band studied previously[18] the CIA spectrum was seen to be composed of essentially eight components, namely those with $\lambda_1\lambda_2\Lambda L$ $=2023$, 0223, 2021, 0221, 2233, 2211, 4045, and 0445. Of

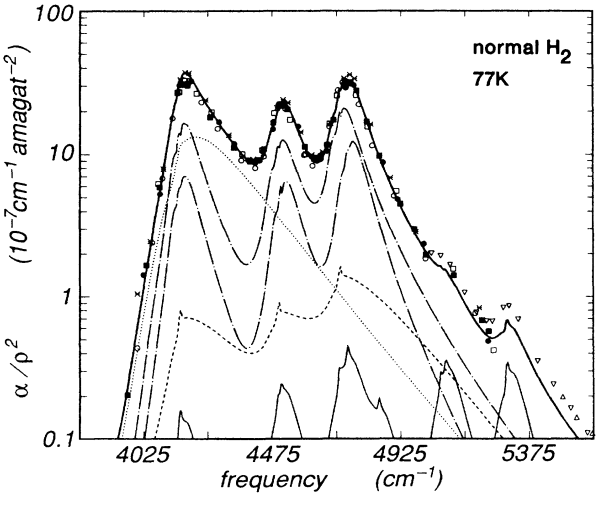

FIG. 8. Binary CIA spectrum at 77 K: calculated from first principles (heavy line). Measurements: dots from Ref. 70; circles from Ref. 73; boxes from Ref. 72; closed squares from Ref. 71; triangles from Refs. 74 and 75. Also shown are intermediate computational results, namely, the $\lambda_1\lambda_2\Lambda L$ components 0001 (dotted); 0223 and 2023 (dot-dashed); 0221 (dashes); 4045 and 0445 (short dash-long dash); and 2233 (thin solid line).

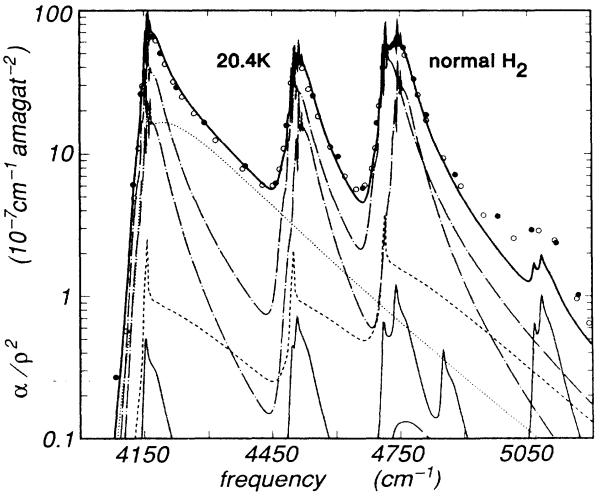

FIG. 10. Binary CIA spectrum at 20.4 K: calculated from first principles (heavy line). Measurements: dots from Ref. 76; circles from Refs. 73 and 77. Also shown are intermediate computational results, namely, the $\lambda_1\lambda_2\Lambda L$ components 0001 (dotted); 0223 and 2023 (dot-dashed); 0221 (dashes); 4045 and 0445 (short dash-long dash); and 2233 (thin solid line).

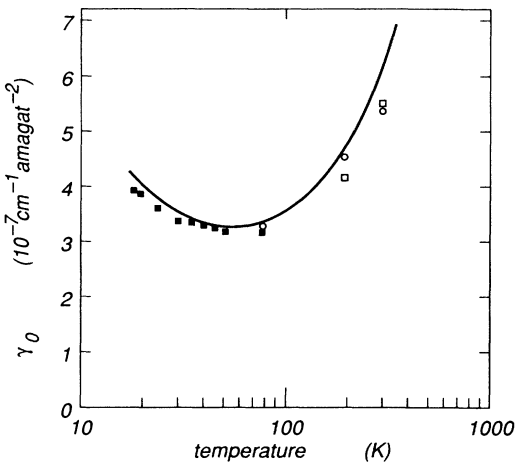

FIG. 11. Computed spectral invariant γ_0 as function of temperature (solid curve) and comparison with measurements in normal hydrogen: ■, from Ref. 72; ○, from Ref. 70; □, from Ref. 71.

these, the three pairs 2023 and 0223, 2021 and 0221, 4045 and 0445, are identical pairs. For the fundamental band, we have another important component, namely, $\lambda_1\lambda_2\Lambda L=0001$ (dotted in the figures) arising from overlap induction. That component is familiar from the CIA spectra of gas mixtures. It occurs here because a vibrating H_2 molecule differs from a nonvibrating one so that a dipole moment exists. Furthermore, the pairs like 2023,0223 mentioned are not identical any more, for the same reason.

At the lower temperatures, especially in Fig. 10, striking features that arise from van der Waals dimers are discernible that have been studied experimentally[1,58–60] and theoretically[61,62] by a number of investigators. We will, therefore, not concern us here with these interesting features.

Figure 11 compares measured and computed spectral invariants γ_0, Eq. (24). Agreement is satisfactory. Theory is generally slightly above measurement, largely because of the intercollisional dip, a region of negative intensity that is absent in our binary theory. As this was concluded from the comparison of theoretical and measured profiles, Fig. 11 shows the general consistency for the spectral invariant as well.

VI. CONCLUSION

The absorption spectra of hydrogen pairs were calculated from first principles, using highly correlated wave functions for the computation of the induced-dipole moment and the vibrational dependences of the isotropic part of the interaction potential. With the expected exceptions of the feeble dimer structures which this work did not attempt to describe, and of the intercollisional dips which arise from higher than binary interactions, the comparison of the measurements with the fundamental theory shows a high degree of consistency. The observed agreement is within the range of experimental uncertainties which we estimate to amount to $\approx 10\%$ for the best measurements presently available. The agreement is as good as this was seen in previous work concerning the rototranslational[15–18] and rotovibrational[23,24] CIA spectra of various molecular pairs. For the simple systems like H_2-H_2, H_2-He, etc., theory is capable of providing CIA spectra with an accuracy comparable to that of the best measurements.

This fact is of interest for various astrophysical studies that require accurate data at temperatures that often differ from those of the laboratory measurements. We have tried to make our work available to interested parties by fitting the computational profiles to simple, analytical functions that can be reproduced on small computers in seconds over a broad range of frequencies and temperatures with simple programming;[67–69] see also a recent review article for further details.[22] Similar work concerned with various vibrational bands of hydrogen pairs is in preparation.

In this work, we have not attempted to exhibit in great detail the effects of the rotational excitations on the induced dipole components B and those of vibrational excitation on the interaction potential because this was done elsewhere for a similar system.[23,24,27,28] The significance of the j,j' corrections is readily seen in the tables and need not be displayed beyond that. The vibrational influence is displayed in Fig. 3; first and second spectral moments show a strong dependence, especially at high temperatures, similar as this was seen earlier for H_2-He,[28] Figs. 4 and 5. The close agreement of the measurements of the RV CIA bands of hydrogen with the fundamental theory shown above certainly depends on the proper accounting for the rotational dependences of the induced-dipole moment, and of the vibrational dependences of the final translational states of the molecular pair.

In conclusion, we remind the reader that previously various theoretical line shapes were compared with measurements of the hydrogen fundamental absorption band on several occasions. The agreement was generally good; see the review articles[1,64] for examples. Given the consistency that was observed in earlier efforts, the reader may wonder what the point of the present work is. A brief comparison of our work with previous effects seems in order.

Previous work of the kind was generally based on empirical induced-dipole models whose parameters were adjusted to fit measured spectra. For molecular systems like hydrogen pairs, empirical dipole models are always simplified, for example, by either suppressing the anisotropic overlap terms, the $\Lambda L=21$ components, in favor of an overlap term in the quadrupole-induced $\Lambda L=23$ components, or else suppressing the overlap term in the 23 component and using instead excessive overlap in the 21 components. The present work is a state-of-the-art description of all significant induced-dipole components; no adjustable parameters appear in this work.

Previous work used empirical model profiles, such as Lorentzians with exponential wings attached which were desymmetrized to satisfy Eq. (1). These profiles were

often matched to theoretical spectral moments, thus providing a "theoretical" spectrum. While such profiles represent the *cores* of induced lines fairly well, they are deficient in the wings.[67] Furthermore, as was mentioned above, Eq. (1) is not the correct symmetry of vibrational profiles; especially the wings of real line profiles deviate significantly as we have seen above. The linear plots usually used for the comparison emphasize the line centers, that is, regions of strong absorption, but a poor representation of the wings (like a 50% discrepancy between theoretical and measured far wings) is hardly noticeable in such plots. On the other hand, we use an exact quantum line shape with most reliable input. In the semilogarithmic plots shown above, a 10% difference between theory and measurement is as discernible near peak absorption as it is in the far wings. In that sense, in the hydrogen fundamental band, theory has not been compared as closely with the measurements before. We note that for the astrophysical applications, an accurate representation of the far wings is of a special significance.

ACKNOWLEDGMENTS

The authors are most grateful to Dr. J. Linsky for his support, and for providing a pleasant working environment for one of us (A.B.). Another author (L.F.) wants to thank Dr. G. Birnbaum for valuable comments after reading the manuscript. The work at the University of Texas was supported by the National Science Foundation, Grant No. AST-86-13085. The authors are also grateful for the support of the Deutsche Forschungsgemeinschaft for an extended visit of one of us (L.F.) in Kaiserslautern. Substantial support for Cray computer time was provided by the University of Texas Center for High-Performance Computing.

*Present address: Department of Physics, Michigan Technological University, Houghton, MI 49931.

[1]H. L. Welsh, *Spectroscopy,* Vol. III of *MTP International Review of Science—Physical Chemistry* (Butterworths, London, 1972), Ser. 1.
[2]J. van Kranendonk, Physica **73**, 156 (1974).
[3]V. N. Filimonov, Usp. Fiz. Nauk. **69**, 565 (1959) [Sov. Phys.—Usp. **2**, 894 (1960)].
[4]G. Birnbaum, L. Frommhold, and G. Tabisz, in *Spectral Line Shapes 5,* edited by J. Szudy (Ossolineum, Warsaw, 1989), p. 623.
[5]N. H. Rich and A. R. W. McKellar, Can. J. Phys. **54**, 486 (1976).
[6]J. L. Hunt and J. D. Poll, Mol. Phys. **59**, 163 (1986).
[7]G. B. Field, W. B. Somerville, and K. Dressler, Ann. Rev. Astron. Astrophys. **4**, 207 (1966).
[8]R. H. Tipping, in *Phenomena Induced by Intermolecular Interactions,* edited by G. Birnbaum (Plenum, New York, 1985), p. 727.
[9]L. Trafton, in *Spectral Line Shapes 5,* edited by J. Szudy (Ossolineum, Warsaw, 1989), p. 755.
[10]J. L. Linsky, Astrophys. J. **156**, 989 (1969).
[11]G. Birnbaum, B. Guillot, and S. Bratos, Adv. Chem. Phys. **51**, 49 (1982).
[12]J. Borysow and L. Frommhold, in *Phenomena Induced by Intermolecular Interactions,* edited by G. Birnbaum (Plenum, New York, 1985), p. 67.
[13]G. C. Maitland, M. Rigby, E. B. Smith, and W. A. Wakeham, *Intermolecular Forces* (Clarendon, Oxford, 1981).
[14]W. Meyer, in *Phenomena Induced by Intermolecular Interactions,* edited by G. Birnbaum (Plenum, New York, 1985), p. 29.
[15]W. Meyer and L. Frommhold, Phys. Rev. A **33**, 3807 (1986).
[16]W. Meyer and L. Frommhold, Phys. Rev. A **34**, 2771 (1986).
[17]W. Meyer and L. Frommhold, Phys. Rev. A **34**, 2936 (1986).
[18]W. Meyer, L. Frommhold, and G. Birnbaum, Phys. Rev. A **39**, 2434 (1989).
[19]J. Schäfer and W. Meyer, in *Electronic and Atomic Collisions,* edited by J. Eichler, I. V. Hertel, and N. Stolterfoht (North-Holland, Amsterdam, 1984), p. 524.
[20]J. Schäfer, Astron. Astrophys. **182**, L40 (1987).
[21]K. L. C. Hunt, in *Phenomena Induced by Intermolecular Interactions,* edited by G. Birnbaum (Plenum, New York, 1985), p. 1.
[22]A. Borysow, L. Frommhold, and P. Dore, Intern. J. Infrared Millimeter Waves **8**, 381 (1987).
[23] L. Frommhold and W.Meyer, Phys. Rev. A **35**, 632 (1987).
[24]A. Borysow, L. Frommhold, and W. Meyer, Phys. Rev. A (to be published).
[25]W. Meyer, Chem. Phys. **17**, 27 (1976).
[26]J. Schäfer and W. Meyer, J. Chem. Phys. **70**, 344 (1979).
[27]M. Moraldi, A. Borysow, and L. Frommhold, Phys. Rev. A **38**, 1839 (1988).
[28]M. Moraldi, J. Borysow, and L. Frommhold, Phys. Rev. A **36**, 4700 (1987).
[29]J. van Kranendonk and R. B. Bird, Phys. Rev. **82**, 964 (1951).
[30]J. van Kranendonk and R. B. Bird, Physica **17**, 953 (1951).
[31]F. R. Britton and M. F. Crawford, Can. J. Phys. **36**, 761 (1958).
[32]R. W. Patch, J. Quant. Spectrosc. Radiat. Transfer **11**, 1311 (1971).
[33]R. W. Patch, J. Quant. Spectrosc. Radiat. Transfer **11**, 1331 (1971).
[34]R. W. Patch, J. Chem. Phys. **59**, 6468 (1973).
[35]R. W. Patch, J. Quant. Spectrosc. Radiat. Transfer **14**, 49 (1974).
[36]J. L. Hunt, J. D. Poll, and L. Wolniewicz, Can. J. Phys. **62**, 1719 (1984).
[37]G. Karl, J. D. Poll, and L. Wolniewicz, Can. J. Phys. **53**, 1781 (1975).
[38]J. D. Poll and J. van Kranendonk, Can. J. Phys. **39**, 189 (1961).
[39]J. D. Poll and J. L. Hunt, Can. J. Phys. **54**, 461 (1976).
[40]J. L. Hunt and J. D. Poll, Can. J. Phys. **56**, 950 (1978).
[41]R. H. Tipping and J. D. Poll, in *Molecular Spectroscopy: Modern Research,* edited by K. N. Rao, (Academic, New York, 1985), Vol. 3, Chap. 7, p. 421.
[42]W. Kolos and L. Wolniewicz, J. Chem. Phys. **43**, 2429 (1965).
[43]W. Kolos and L. Wolniewicz, J. Chem. Phys. **49**, 404 (1968).
[44]W. Kolos and L. Wolniewicz, J. Molec. Spectrosc. **54**, 303 (1975).
[45]J. van Kranendonk, Physica **24**, 347 (1958).
[46]W. Kolos and L. Wolniewicz, J. Chem. Phys. **46**, 1426 (1967).
[47]J. D. Poll and L. Wolniewicz, J. Chem. Phys. **68**, 3053 (1978).
[48]T. Lorenz and W. Meyer (unpublished).
[49]G. C. Maitland, M. Rigby, E. B. Smith, and W. A. Wakeham,

Intermolecular Forces (Clarendon, Oxford, 1981).
[50]W. Meyer (unpublished).
[51]J. Schäfer, Z. Phys. D (to be published).
[52]W. Meyer (unpublished).
[53]J. Schäfer and L. Monchick, J. Chem. Phys. **87**, 171 (1987).
[54]J. Schäfer, Astron. Astrophys. **182**, L40 (1987).
[55]J. Schäfer and A. R. W. McKellar (unpublished).
[56]G. Birnbaum, S. Chu, A. Dalgarno, L. Frommhold, and E. L. Wright, Phys. Rev. A **29**, 595 (1984).
[57]M. Moraldi, A. Borysow, and L. Frommhold, Chem. Phys. **86**, 339 (1984).
[58]A. R. W. McKellar and H. L. Welsh, Can. J. Phys. **52**, 1082 (1974).
[59]D. K. Rank, B. S. Rao, P. Sitaram, A. F. Slomba, and T. A. Wiggins, J. Opt. Soc. Am. **52**, 1004 (1962).
[60]A. Watanabe and H. L. Welsh, Phys. Rev. Lett. **13**, 810 (1964).
[61]R. G. Gordon and J. K. Cashion, J. Chem. Phys. **44**, 1190 (1966).
[62]L. Frommhold, R. Samuelson, and G. Birnbaum, Astrophys. J. **283**, L79 (1984).
[63]J. Schäfer, in *Spectral Line Shapes 5,* edited by J. Szudy (Ossolineum, Warsaw, 1989), p. 807.
[64]S. P. Reddy, in *Phenomena Induced by Intermolecular Interactions,* edited by G. Birnbaum (Plenum, New York, 1985), p. 129.
[65]J. van Kranendonk, Can. J. Phys. **46**, 1173 (1968).
[66]J. C. Lewis, in *Phenomena Induced by Intermolecular Interactions,* edited by G. Birnbaum (Plenum, New York, 1985), p. 215.
[67]J. Borysow, L. Trafton, L. Frommhold, and G. Birnbaum, Astrophys. J. **296**, 644 (1985).
[68]A. Borysow, L. Frommhold, and M. Moraldi, Astrophys. J. **336**, 495 (1989).
[69]A. Borysow and L. Frommhold, Astrophys. J. **341**, 549 (1989).
[70]J. L. Hunt, Ph.D. thesis, University of Toronto, 1959.
[71]S. P. Reddy, G. Varghese, and R. D. G. Prasad, Phys. Rev. A **15**, 975 (1977).
[72]A. Watanabe, Ph.D. thesis, University of Toronto, 1964.
[73]A. Watanabe and H. L. Welsh, Can. J. Phys. **43**, 818 (1965).
[74]S. P. Reddy, A. Sen, and R. D. G. Prasad, J. Chem. Phys. **72**, 6102 (1980).
[75]A. Sen, R. D. G. Prasad, and S. P. Reddy, J. Chem. Phys. **72**, 1716 (1980).
[76]A. Watanabe, Can. J. Phys. **49**, 1320 (1971).
[77]A. Watanabe and H. L. Welsh, Can. J. Phys. **45**, 2859 (1967).